Article

CO Oxidation at Near-Ambient Temperatures over TiO$_2$-Supported Pd-Cu Catalysts: Promoting Effect of Pd-Cu Nanointerface and TiO$_2$ Morphology

Abdallah F. Zedan [1],*, Safa Gaber [2], Amina S. AlJaber [3] and Kyriaki Polychronopoulou [2,4],*

[1] National Institute of Laser Enhanced Science, Cairo University, Main Campus, Giza 12613, Egypt
[2] Center for Catalysis and Separations, Khalifa University of Science and Technology, Abu Dhabi P.O. Box 127788, United Arab Emirates; saagaber90@gmail.com
[3] Department of Chemistry, Qatar University, Doha 2713, Qatar; a.s.aljaber@qu.edu.qa
[4] Department of Mechanical Engineering, Khalifa University of Science and Technology, Abu Dhabi P.O. Box 127788, United Arab Emirates
* Correspondence: azedan@niles.edu.eg (A.F.Z.); kyriaki.polychrono@ku.ac.ae (K.P.); Tel.: +20-2-35675236 (A.F.Z.)

Abstract: Significant improvement of the catalytic activity of palladium-based catalysts toward carbon monoxide (CO) oxidation reaction has been achieved through alloying and using different support materials. This work demonstrates the promoting effects of the nanointerface and the morphological features of the support on the CO oxidation reaction using a Pd-Cu/TiO$_2$ catalyst. Pd-Cu catalysts supported on TiO$_2$ were synthesized with wet chemical approaches and their catalytic activities for CO oxidation reaction were evaluated. The physicochemical properties of the prepared catalysts were studied using standard characterization tools including SEM, EDX, XRD, XPS, and Raman. The effects of the nanointerface between Pd and Cu and the morphology of the TiO$_2$ support were investigated using three different-shaped TiO$_2$ nanoparticles, namely spheres, nanotubes, and nanowires. The Pd catalysts that are modified through nanointerfacing with Cu and supported on TiO$_2$ nanowires demonstrated the highest CO oxidation rates, reaching 100% CO conversion at temperature regime down to near-ambient temperatures of ~45 °C, compared to 70 °C and 150 °C in the case of pure Pd and pure Cu counterpart catalysts on the same support, respectively. The optimized Pd-Cu/TiO$_2$ nanowires nanostructured system could serve as efficient and durable catalyst for CO oxidation at near-ambient temperature.

Keywords: heterogeneous catalysis; carbon monoxide; palladium; copper; titania; nanointerface; morphology

1. Introduction

The catalytic oxidation of carbon monoxide (CO) to carbon dioxide (CO$_2$) over supported metal catalysts has been considered one of the most efficient technologies to remove toxic CO pollutants from the environment [1–4]. Among the different studied catalytic systems, palladium-based nano catalysts have shown excellent catalytic activity for the CO oxidation reaction in the absence and presence of hydrogen [5–8]. However, palladium by itself is an expensive and rare metal. Therefore, great research efforts have been devoted to the improvement of the catalytic activity and stability of the Pd-based catalysts toward the low-temperature CO oxidation [9]. To achieve this goal, several strategies have been investigated including alloying [10,11] or coupling different plasmonic materials, development of bimetallic catalysts [12] using different support materials [9,12] hence increasing the porosity of the support [13,14] and improving the metal–support interaction [10,15] as well as nanointerfacing. The metal–support interaction was found to contribute to higher catalytic activity through enhanced metal dispersion and stability. At the same time, establishing nanointerface between Pd and other metals has been shown

as a promising way for improving the catalytic activity toward CO oxidation at low or ambient temperatures [16,17]. When it comes to the support, TiO_2-based nanomaterials have been widely used as catalytic support in several environmental applications including CO removal [1,18,19]. The TiO_2 support is known for its high surface area, outstanding chemical stability under reducing and oxidizing conditions, and capability to provide an oxygen-transport medium in the gas-solid reactions [20–22].

This study focuses on the rational synthesis of TiO_2-supported Pd-Cu catalysts and modulating their associated CO conversion temperatures by tailoring the Pd-Cu interface and the TiO_2 morphology for enhanced activity in CO oxidation. The synthesis of the active Pd-based catalysts was based on a two-step wet impregnation of the Pd and Cu nanoparticles onto previously prepared TiO_2 support of three different morphologies, namely nearly nanospheres, nanotubes, and nanowires to probe the effects of the Pd-Cu interface and the TiO_2 properties on the surface reactivity and CO oxidation rates. Here, we demonstrate that Pd-Cu nano interfacing while using TiO_2 support could increase the metal–support interaction and enhance the catalytic activity for CO oxidation at near-ambient temperatures and thus raising the catalyst's potential in practical applications.

2. Materials and Methods

2.1. Materials

Chemicals and reagents were purchased from Sigma-Aldrich (Taufkirchen, Germany) and used without further purification, including titanium (IV) oxide spherical particles (TNS, anatase, −325 mesh powder, ≥99% trace metals basis, Sigma-Aldrich), sodium hydroxide (pellets, anhydrous, ≥98%, Sigma-Aldrich), potassium hydroxide (reagent grade, ≥98%, Sigma-Aldrich), hydrochloric acid (ACS reagent, 37%, Sigma-Aldrich), copper (II) nitrate trihydrate (purum, 98%, Sigma-Aldrich), ammonium carbonate (ACS reagent, 99%, Sigma-Aldrich), and palladium (II) nitrate solution 10 wt. % in 10 wt. % nitric acid (99.99% trace metal basis, Sigma-Aldrich). The water used was ultrapure deionized water (Direct-Q 5UV/Millipore, Molsheim, France).

2.2. Methods

2.2.1. Synthesis of Titania Nanotubes (TNT) and Titania Nanowires (TNW)

The titania (TiO_2) nanotubes (TNT) and nanowires (TNW) were prepared by the strong alkaline treatment of spherical anatase TiO_2 particles under hydrothermal conditions followed by the acidic treatment using diluted HCl solution, as reported earlier [19,23].

Titania nanotubes (TNT): For the synthesis of titania nanotubes (TNT), 2 g of TiO_2 anatase spherical (TNS) particles were mixed with 40 mL of 10 M aqueous NaOH solution in a 100 mL Teflon vessel. The mixture was stirred for 30 min at ambient temperature and pressure. The Teflon vessel containing the mixture was placed inside a stainless-steel autoclave reactor and was then transferred to an electric oven (Isotemp, Fisher-Scientific, Marietta, OH, USA). The autoclave reactor was kept in the electric oven at 140 °C for 48 h. Upon completion, the hydrothermal products were separated by filtration and rinsed thoroughly with deionized water several times. Then, the products were soaked in an aqueous solution for 2 h at room temperature after adjusting the pH to 6 with 0.1 M HCl. Finally, the products were separated by filtration and were dried in an electric oven at 80 °C for 24 h. The dried powder samples were calcined in a muffle furnace (Nebertherm, Bremen, Germany) under static air at 450 °C for 2 h with a heating rate of $5° \, min^{-1}$.

Titania nanowires (TNW): For the synthesis of the titania nanowires (TNW), a procedure typical to that used for the synthesis of TNT was followed except using 10 M aqueous potassium hydroxide (KOH) as an alkaline agent for the hydrothermal treatment. All other steps including separation, purification, acidic treatment, drying, and calcination were the same as the TNT samples. The TiO_2 different shaped supports are coded as TNS, TNT, and TNW in the following sections.

2.2.2. Synthesis of Copper/Titania (Cu/TiO$_2$) Catalysts

The copper/titania catalysts with different-shaped titania supports were generally prepared by the homogenous deposition precipitation using ammonium carbonate as a precipitating agent and followed by high-temperature calcination of purified and dried products. The different Cu/TiO$_2$ catalysts were synthesized using the same loading of 2 wt. % Cu on TiO$_2$ of various shapes (nanospheres, nanotubes, and nanowires). The catalysts that were prepared were namely 2 wt. % Cu/TNS, 2 wt. % Cu/TNT, and 2 wt. % Cu/TNW. In a typical synthesis of each of the Cu/TNS, Cu/TNT, and Cu/TNW, about 600 mg of TNS, TNT, and TNW were separately dispersed in a 40 mL deionized water by stirring and ultrasonication in an Erlenmeyer flask. A pre-determined volume of an aqueous solution of copper II nitrate-trihydrate (Cu (NO$_3$)$_2$.3H$_2$O) was added to the respective titania-water suspension to give a final nominal loading of 2 wt. % Cu on various-shaped titania supports. The aqueous Cu^{2+}/TiO$_2$ reaction mixture was aged at ambient temperature for 12 h under continuous mechanical stirring followed by a drop-wise addition of an aqueous solution of 0.5 M ammonium carbonate ((NH$_4$)$_2$CO$_3$) till the pH of the mixture reached ~9. Then the reaction mixture was stirred under mild temperature of 70 °C for 6 h. The resulting precipitated products were separated by centrifugation and were washed three times with deionized water. Finally, the obtained precipitates were dried at 80 °C for 12 h followed by calcination in a closed muffle furnace at 400 °C for 2 h with a heating ramp rate of 5° min^{-1}.

2.2.3. Synthesis of Palladium-Copper/Titania (Pd-Cu/TiO$_2$) Catalysts

The different palladium-copper/titania catalysts were prepared using the controlled deposition precipitation method followed by the high-temperature calcination. The different palladium-copper/titania catalysts contained fixed amounts of 5 wt. % Pd and 2 wt. % Cu loaded onto various-shaped TiO$_2$ (nanospheres, nanotubes, and nanowires) particles. The prepared palladium-copper/titania catalysts were coded as Pd-Cu/TNS, Pd-Cu/TNT, and Pd-Cu/TNW. These catalysts were generally synthesized as follows: for each catalyst, about 0.5 g of Cu/TNS, Cu/TNT, and Cu/TNW was separately suspended in a 50 mL deionized water by stirring and ultrasonication. Then, a pre-determined volume of palladium (II) nitrate solution 10 wt. % in 10 wt. % nitric acid (Pd (NO$_3$)$_2$/HNO$_3$) was added to the respective Cu/titania aqueous suspension to give a final nominal loading of 5 wt. % Pd on various-shaped 2% Cu/titania. The aqueous Pd^{2+}/Cu/TiO$_2$ reaction mixture was aged at ambient temperature for 12 h under continuous mechanical stirring after a drop-wise addition of an aqueous solution of 0.2 M sodium hydroxide ((NaOH) till the pH of the mixture reached ~9. The resulting precipitated products were separated by centrifugation and were washed three times with deionized water. The obtained precipitates were dried at 80 °C for 12 h and were finally calcined in a closed muffle furnace at 400 °C for 2 h with a heating ramp rate of 5° min^{-1} to obtain the powder catalysts. For the sake of comparison different Pd/titania catalysts with fixed loading of 5 wt. % Pd on various-shaped TiO$_2$ particles (Pd/TNS, Pd/TNT, and Pd/TNW) were prepared using the above-mentioned procedure. The deposition precipitation of Pd was performed over pure TiO$_2$ nanospheres, nanotubes, and nanowires instead of copper/titania particles. The same procedure for purification and calcination was followed. All prepared calcined catalysts were kept for characterization and further catalysis measurements.

2.3. Catalysts Characterization

The prepared catalysts were characterized using different techniques as it is described below.

NOVA NANOSEM 450 (FEI, Brno, Czech Republic) was used to collect scanning electron microscopy (SEM) images. The sample under study was coated with thin layer of gold to avoid charging effect. X-ray diffraction (XRD) spectra were collected using MiniFlex II powder diffraction system (Rigaku, Tokyo, Japan) with Cu Kα radiation (λ = 1.54056 Å). The analysis was done with diffractometer at a voltage of 30 kV and intensity of 20 mA

with scanning speed of 0.025°/step/second. The average crystallite size was calculated using Scherrer equation $D = \frac{k \lambda}{\beta \cos \theta}$, where D indicates the average crystallite size, K = 0.9 (shape factor), λ is the X-ray wavelength, θ is the X-ray reflection angle, and β is the full width at half-maximum (FWHM) of the diffraction peak (radians) [24–26]. Nitrogen adsorption and desorption isotherms were collected on ASAP 2460 pore size analyzer (Micromeritics, Norcross, GA, USA) (at 77 K) and recorded in the range of 0.05 to 1 relative pressure. The specific surface area was calculated based on the BET (Brunauer-Emmett-Teller) method. The samples were degassed at 90 °C for 1 h then at 150 °C for 1 h using N_2-He mixture before the physisorption analysis. X-ray photoelectron spectroscopy (XPS) analysis was performed to give an insight to the oxidation state and chemical environment at the surface of the catalyst. KRATOS AXIS Ultra XPS (KRATOS Analytical, Manchester, UK) spectroscopy was used and equipped with a monochromatic Al Kα radiation source (hv = 1486.6 eV) in chamber at ca. 5×10^{-9} Torr base pressure. The high-resolution core level spectra measurement was done at high-resolution pass energy of 20 eV, 10 mA emission current, and 15 kV anode HT. The C1s peak was used for calibration and correcting the surface charging effect. Raman analysis was conducted using 780 nm laser sources in DXR 2 Raman Microscope (Thermo-Fisher Scientific, Madison, WI, USA). The analysis was done at 5 mW power and 4 cm^{-1} spectral resolution.

2.4. Catalytic Activity and Stability

The catalytic activity of the prepared catalysts was evaluated toward the CO oxidation reaction. A fixed bed catalytic reactor including a quartz tube of 10 mm inner diameter was used. The details of CO oxidation experiments are described in our previous works [4,27,28]. In each experiment, 50 mg catalyst was loaded and then placed in the middle of a programmable split tube furnace (Lindberg/Blue M Mini-Mite, Thermo Fisher Scientific, Waltham, MA, USA) under atmospheric pressure. In a typical catalysis measurement, a feed gas comprising 4% CO and 20% O_2 (with Ar as a balance) and having a flow rate of 60 cm^3/min (72,000 cm^3 g^{-1} h^{-1} WHSV) was introduced into the bed. Effluents of the bed were analyzed using an infrared gas (IR) analyzer (IR200, Yokogawa, Japan). The surface temperature of the catalyst bed was raised with 5 °C/min ramping and monitored through in situ *k*-type thermocouple. The percentage volume of the CO and O_2 as reactants, CO_2 as a product as well as the temperature were recorded simultaneously using custom-configured program based on the LabVIEW data acquisition software (Version 14.0F1, National Instruments, Austin, TX, USA). The long-term stability of the selected catalyst was evaluated at 60 ± 5 °C for 72 h under continuous feed gas. The percentage of CO conversion was calculated from the equation, X_{CO} (%) = $\frac{[CO]_{in} - [CO]_{out}}{[CO]_{in}} \times 100$, where X is the percentage conversion and [CO] is the CO molar flow in the inlet/ outlet feed gas.

3. Results and Discussion

3.1. Morphological Features

Scanning electron microscopy (NOVA NANOSEM 450, Brno, Czech Republic) was used to observe the morphology of the different TiO_2 supports and the influence of the surface morphology on the Pd-Cu incorporation. Figure 1 shows the morphology of (a) TiO_2 sphere (b) TiO_2 nanotube, (c) TiO_2 nanowire, and (d-e) Pd-Cu–TiO_2, nanowire. The TiO_2 sphere (Figure 1a) are loosely agglomerating with an average particle size of around 115 nm. Figure 1b shows a uniform nanotubular morphology with an average diameter of 29 nm and few micrometer lengths. The nanowire (Figure 1c) shows an ultra-fine well separated wire morphology with a diameter of ~45 nm and a length of several micrometers. Comparing (Figure 1c) with (Figure 1d,e), it can be seen that the nanowire morphology changed after Pd and Cu addition, where the wire length became shorter adopting a more flake-like morphology. It was possible to identify the elements present in the catalytic system through EDX analysis (Figure 1f), where peaks associated with Cu, Pd, Ti, and O in absence of any other impurity were found. In addition, from the measured elemental composition analysis, the loaded metals were identified to be 4.2 wt.% for Pd and 2.2 wt.%

for Cu which is close enough to the theoretical (nominal) metal loading (5 wt.% for Pd and 2 wt.% for Cu). This shows that no loss, due to e.g., leaching, happened during the synthesis and/or the calcination steps. Regarding the slight excess of O_2 compared to the wt.% (EDX) required by TiO_2, this could be due to the presence of Pd and Cu oxide. In addition, it should be kept in mind that EDX is not quite ideal for the quantification of light elements like oxygen, so some contribution of the intrinsic deficiency of the EDX technique cannot be excluded.
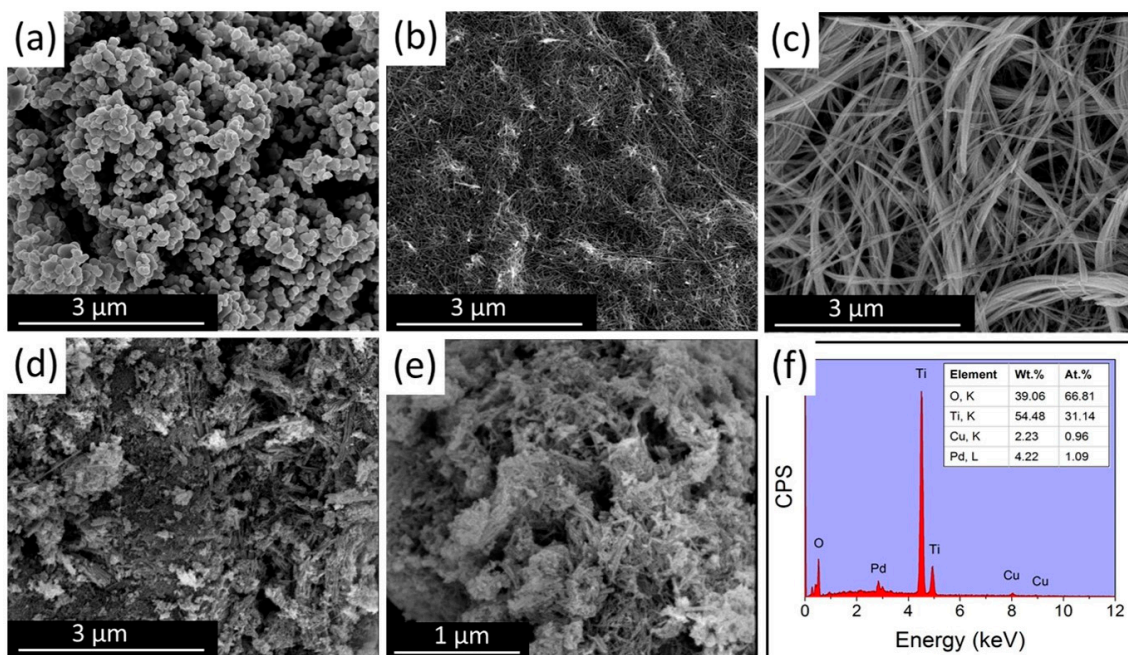

Figure 1. SEM images of (**a**) TiO_2 sphere; (**b**) TiO_2 nanotube; (**c**) TiO_2 nanowire; (**d**,**e**) Pd-Cu–TiO_2 nanowire catalyst; and (**f**) elemental analysis of Pd-Cu/TiO_2 nanowire catalyst.

3.2. Crystal Structure

The crystallinity of the different catalysts was investigated using X-ray diffraction and the results are presented in Figure 2A. As it can be seen, all the major characteristic peaks coincide well with TiO_2 anatase phase. In particular, the main peaks at around 25.3, 37.6, 47.9, 53.7, 55.0, and 62.2 2theta values can be assigned to (101), (004), (200), (105), (211), and (204) reflections of the anatase phase, respectively. All these peaks correlate well with the Joint Committee on Powder Diffraction standard (JCPDS No. 21-1272) for the TiO_2 anatase phase [29–31]. In general, in all of the prepared catalysts, the crystal structure was maintained after mono (Cu or Pd) and bimetallic (Cu-Pd) addition on the titanium oxide support, in any of the studied morphologies, was performed. Comparing the XRD pattern with literature and our previously reported XRD pattern of anatase TiO_2, it can be found that addition of Cu on the different supports, does not result in any CuO peaks formation. The XRD patterns show no distinguished diffraction peak for CuO, metallic phase of Cu or Pd or their Pd-Cu alloy, maybe due to the fact that the studied metal loading is relatively low (5 wt. % Pd and 2 wt. % Cu) or the final size is too small to be detected. The presence of a small peak at 2θ = 27.32°, in some cases, such as in the Cu/TNS catalyst, has been linked to rutile phase impurities as it corresponds to (110) crystal plane of rutile phase of titanium oxide (JCPDS Card no. 21-1276) [29,32]. In all of the herein prepared catalysts, a slight upshift was found in the main (101) 2θ value peak compared to pure TiO_2 (Figure 2B). Similar shift was reported by Ahmad et al. in their study of bimetallic palladium-supported halloysite nanotubes [12]. This shift can be attributed to the decrease

in the values of lattice constant (lattice unit cell reduction) upon partial metal incorporation that cannot be excluded [12].
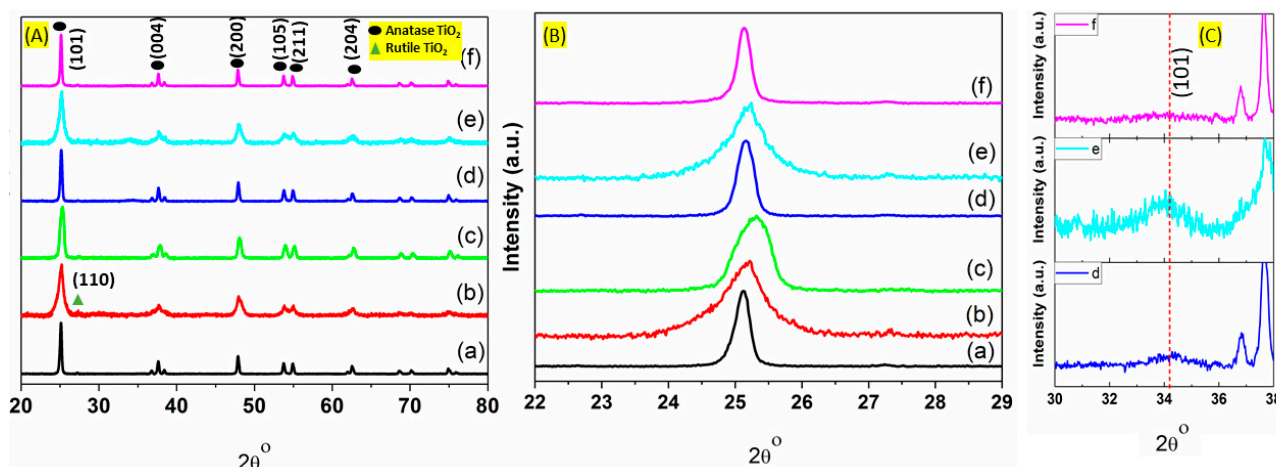

Figure 2. (**A**) XRD patterns of (a) Cu-TNS, (b) Cu-TNT, (c) Cu-TNW, (d) Pd-Cu-TNS, (e) Pd-Cu/TNT, (f) Pd-Cu/TNW catalysts. (**B**) TiO$_2$ anatase (101) reflection of the catalysts in (**A**); (**C**) PdO (101) reflection for the (d–f) catalysts of (**A**).

The crystallite sizes of anatase TiO$_2$ were determined based on the diffraction peak at (101) plane using Scherrer's equation (Figure 2B). The results are summarized in Table 1 and were found to be 29.5 nm, 9.2 nm, and 14.1 nm for Cu/TNS, Cu/TNT, and Cu/TNW, respectively. The further addition of the second metal, Pd, to the system results in an increase in the relative crystallite size in titanium nanotube and nanowire morphology cases, as the size increases to 13.9 nm for Cu/TNT and up to 32.1 nm for Cu/TNW. Yao et al. reported similar observation in their study of CuO addition to the outer surface of titanium oxide nanotube [33]. However, it is worth mentioning that the crystallite size increases largely in the titanium oxide with nanowire morphology (TNW case). As a result, the width of the peak assigned to the (101) plane becomes narrow and sharp when Pd was introduced. This can indicate that Pd addition can induce structural and surface changes; the latter can vary with the structural morphology of the support. Mostly, it is believed that Pd addition may display a preferential growth along the in-plane axis of the nanowire TiO$_2$. On the other hand, the addition of Pd to the titanium oxide nanosphere (TNS case) resulted in slight decrease in the crystallite size (27.6 nm), may be due to the crystal growth interruption by the Pd introduction on the titanium oxide sphere. A decrease in crystallite size upon doping of different metals, Cu^{2+}, Zn^{2+}, and Fe^{2+} in the titanium oxide was previously reported [34,35]. In general, we can reasonably conclude that different morphologies induce different response in the system upon Pd addition, due to varying solution species diffusivity and differences in the solute species solid surface contact area, spheres, nanowires, and nanotubes are expected to have different contact areas for the anchoring of the species coming from the solution. This process is expected to lead to different metal-support interface/interactions, affecting the subsequent catalysis taking place.

Table 1. Textural properties along with crystallite size of different prepared catalysts of this study.

Catalyst	Crystal Size (nm) *	Surface Area (m^2/g)	Pore Volume (cm^3/g)
Cu-TNS	29.5	-	-
Cu-TNT	9.2	-	-
Cu-TNW	14.1	38.1	0.83
Pd-Cu/TNS	27.6	-	-
Pd-Cu/TNT	13.9	-	-
Pd-Cu/TNW	32.1	34.6	0.62

* by applying Scherrer equation on the measured from TiO$_2$ (101) peak based on Scherrer formula.

Compared to the monometallic systems, the presence of palladium in the Cu/TiO_2 catalyst (bimetallic system) leads to the appearance of a small peak at around $2\theta = 34.4°$ as can be seen in (Figure 2C). This peak can be assigned to (101) reflection of PdO phase (PdO, JCPDS 41-1107) [36,37]. Using Scherrer's equation, the crystallite size of PdO was found to be ~6.7 nm. The PdO peaks appearance can be attributed to the fact that Cu presence is not expected to facilitate the complete reduction of Pd^{2+} to Pd^0, in the absence of a reducing agent (e.g., hydrogen) in the bimetallic TiO_2 catalysts. This explanation agrees well with similar studies on bimetallic photocatalysts $Pd–Cu/TiO_2$ by P. Lisowski and his group [38]. However, it should be noted that this is not the case for Pd/Cu on TNW where the PdO peak almost disappear (see Figure 2C). This could be explained by the fact that nanowire TiO_2 has high surface to volume ratio and long axial morphology which mean more exposed surface available for Pd-Cu interaction which is expected to facilitate the reduction of Pd^{2+} [39]. This nano interfacial morphology leads to well dispersion of the Pd metal on the crystal lattice of titanium oxide. It should be mentioned that the absence of metallic Pd (111) peak at $2\theta = 40°$ (Pd, JCPDS 05-0681), could be explained by the high dispersion of metal particles that escape the XRD detection; TEM analysis would assist on that front [37].

3.3. Textural Analysis

The N_2 adsorption/desorption isotherms for selected mono- and bi-metallic catalysts, namely Cu-TNW and Pd-Cu-TNW are presented in Figure 3. Both catalysts show type IV isotherms and H3 hysteresis loop indicating mesoporous structure with pore width in the range of 2–50 nm according to IUPAC classification [33,40]. The hysteresis loop appearing in the multilayer range of physisorption isotherms is attributed to capillary condensation taking place in the mesopores [41]. Generally, it can be seen that there is no change in the shape of the isotherm for both catalysts, as we move from Cu to the Pd-Cu system, compared to TiO_2 P25 isotherm previously reported in our study of CuO-TNT [19]. This indicates that the support maintained its pore structure upon Cu or Pd/Cu addition.
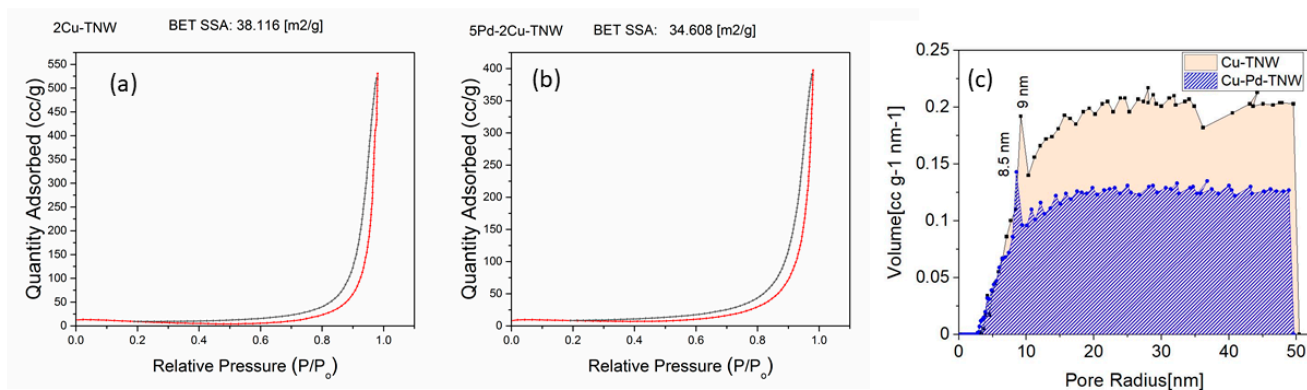

Figure 3. N_2 adsorption–desorption isotherms over (**a**) Cu-TNW; (**b**) Pd-Cu-TNW catalysts; (**c**) BJH pore size distribution.

However, as expected, the BET surface area exhibited a slight decrease upon metal introduction. The further addition of Pd, led to a further decrease in the surface area. The surface area of Cu-TNW and Pd-Cu-TNW were found to be 38.1 and 34.6 m^2/g, respectively (Table 1). This is an expected pattern and can be attributed to the pore filling by the added Cu^{2+} and Pd^{2+} which are incorporated and entrapped in the cavities of the support [9,12]. Similar decrease of BET surface area upon metal doping was reported by De Queiroz et al. and Wang et al. in their study of $Cu/TiO_2–Cu/Al_2O_3$ catalysts and $Pd/Cu/MOx$ (MOx=TiO_2 and Al_2O_3) catalysts, respectively [9,40]. Hossain et al. also shows that both pore volume and surface area decreased upon incorporation of Cu in the titanium nanotube structure [29]. BJH size distribution in (Figure 3c) shows that Cu-TNW

and Pd-Cu/TNW poses major size peak at around 9 nm with 0.83 and 0.62 cc/g total pore volume, respectively.

3.4. Surface Properties

XPS was used to further investigate the chemical environment at the surface of the catalysts and understand the oxidation state of the different elements. The XPS core level (high resolution, HR) spectra of Ti 2p, O 1s, Pd 3d, and Cu 2p are shown in Figure 4 for Cu-Pd/TNS, Cu-Pd/TNT, and Cu-Pd/TNW. The HR-XPS scan for the Ti 2p in the different TiO_2 was acquired from 450 to 477 eV. For Cu 2p and O 1s, the HR-XPS scan was acquired from 925 to 980 eV and from 525 to 540 eV, respectively. While for Pd 3d, the scan was collected from 335 to 350 eV. The binding energy of the peaks can be found in Table S7.
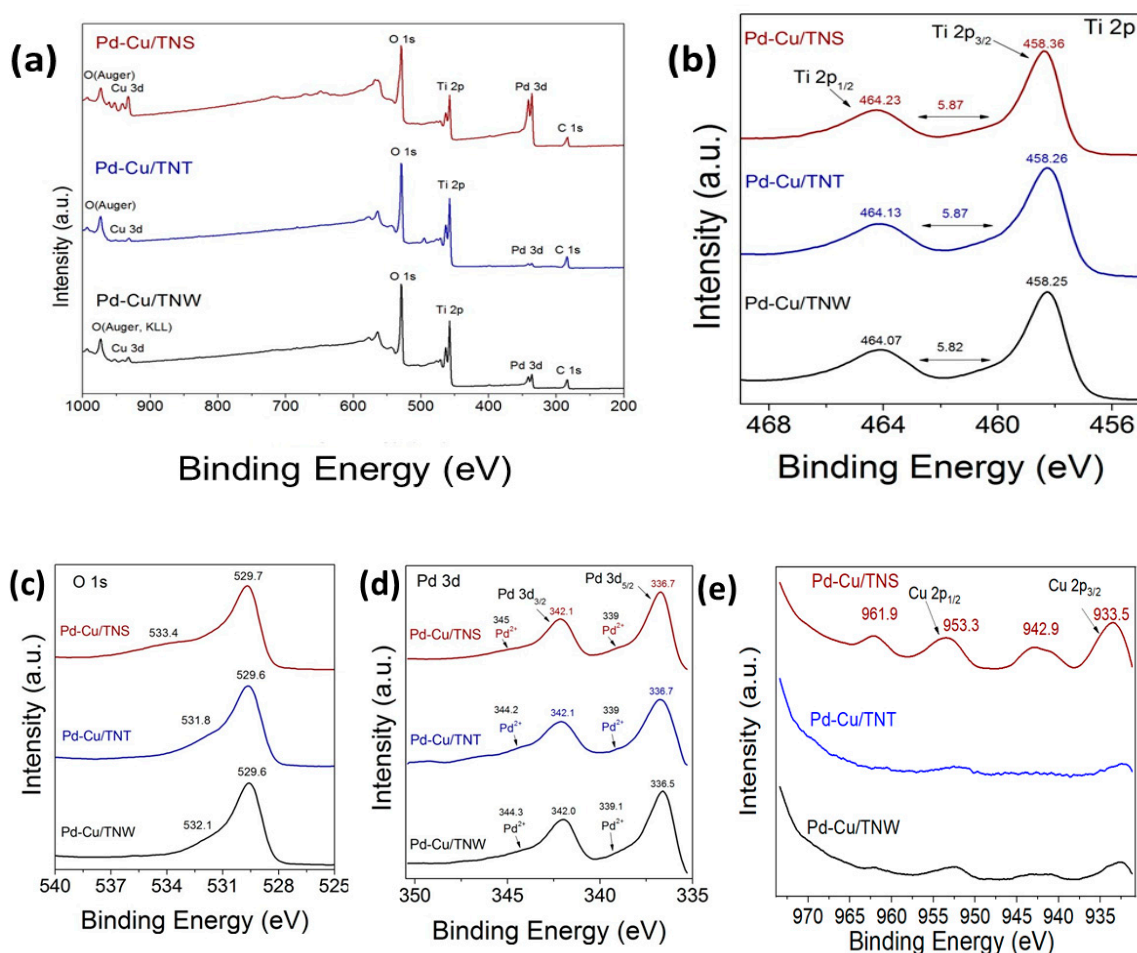

Figure 4. (**a**) Survey XPS spectra obtained over the Pd-Cu/TNS, Pd-Cu/TNT, and Pd-Cu/TNW catalysts; high-resolution XPS spectra over Pd-Cu/TNS, Pd-Cu/TNT, and Pd-Cu/TNW catalysts; (**b**) Ti 2p; (**c**) O 1s, (**d**) Pd 3d, and (**e**) Cu 2p core level spectra.

High resolution spectrum of Ti 2p region of Pd-Cu/TiO_2 (Figure 4b), revealed two peaks at 458.25 eV in TNW and 458.26 eV in TNT and a second peak at 464.07, 464.13 for TNW and TNT support system, respectively. Similarly, Pd-Cu/TNS shows two peaks at 458.36 and 464.23 eV. Those two peaks are assigned to Ti $2p_{3/2}$ and Ti $2p_{1/2}$ at the higher binding energy side. A very slight shift can be observed especially in TNW- and TNT-based catalyst compared to TiO_2 alone. The observed shift of the order of 0.04/0.05 eV toward lower binding energy (BE) can be attributed to oxygen vacancy generation and Ti^{3+} formation upon reduction due to the presence of copper. This structural disorder due to Cu addition can also be confirmed by the XRD studies (Figure 2B) and the shape change of

the (101) peak of anatase. The down shift in Ti 2p peaks was also reported by Cheng-Yen Tsai and Deng et al. in their study of Cu-doped TiO_2 and CuO supported on CeO_2-doped TiO_2, respectively [42,43] and shows similar trend with our previous work [19]. In addition, it can be clearly seen that the distance between the main Ti $2p_{3/2}$ and Ti $2p_{1/2}$ is about 5.87 eV in all of the different-shaped TiO_2-based catalysts, indicating that TiO_2 structure of the support is preserved upon the addition of metals [19].

The high resolution XPS spectra of Pd (3d) core level of the three Pd-Cu/ TiO_2 catalysts presented in Figure 4d, are featured with two (2) main peaks centered at around 337.1 and 342.5 eV, that can be attributed to metallic Pd in $3d_{5/2}$ and $3d_{3/2}$ regions, while the other two peaks observed at around 338.3 and 343.7 eV, are assigned to Pd^{2+} species most likely in PdO (in agreement with the XRD findings) [11]. The overlapped peaks were fitted by Gaussian curves [11]. The details of the peak fitting analysis can be found in the Supplementary Tables S1–S3 and Figure 5. In the Pd $3d_{5/2}$ and $3d_{3/2}$ regions, a clear positive shift toward higher binding energy was observed in all the prepared catalysts of this study. Compared to Pd binding energy reported in literature [44], around 1.3 eV upshift demonstrate the strong Pd interaction with the TiO_2 support. This is similar to what have been observed in other studies of Pd incorporation [11,12,45,46]. Furthermore, the formation of Cu-Pd alloy can enhance the shifting of the binding energy. The shift in the binding energy of Pd in bimetallic system compared to monometallic was explained by the induced modification in the electronic structure of the valence d band [46].
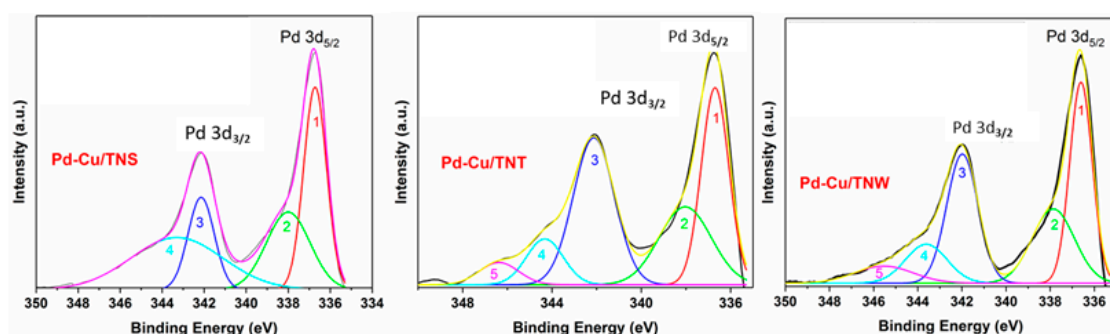

Figure 5. Peak deconvolution for Pd 3d for Pd-Cu/TNS, Pd-Cu/TNT, and Pd-Cu/TNW.

As can be seen in Figure 4e, high resolution XPS spectrum of the Cu(2p) core level region of the Cu-Pd/ TiO_2 indicate Cu $2p_{3/2}$ and Cu $2p_{1/2}$ core peaks. The peak deconvolutions revealed the presence of four (4) main peaks. The peak located at ~933.5 eV corresponds to Cu^{2+}, while strong peaks at around 942.9 and 961.9 eV can be assigned to Cu^{2+} (CuO phase). The other shakeup satellite peaks at 950–960 eV and 940–945 eV, can be attributed to the presence of unfilled 3d or multielectron excitation as reported in other studies of Cu [12,47,48] and it can be used as an indication of Cu^{2+} presence [48,49]. The peak expected at 953 eV combined with the weak satellite peak indicate the presence of Cu^+. Overall, it can be observed that Cu 2p peaks in all Cu-Pd/ TiO_2 catalysts shifted to higher binding energy in comparisons to CuO alone [19]. The presence of the support, lead to peak shifting to higher binding energy which can reflect the effect of strong metal-support interaction at the catalyst interface. The location of the Cu $2p_{3/2}$ and Cu $2p_{1/2}$ binding energy are comparable to other similar catalysts prepared by Yahia H. Ahmad and Wenliang Gao et al. [12,50] and indicate the presence of both Cu^{2+} and Cu^+.

However, it should be noted that this upshift might be counteracted to some extent by the palladium addition. Chiba et al. in their study of Cu-Pd nanoparticles reported as the palladium ratio increased, Cu $2p_{3/2}$, shifts to lower binding energy [46]. The downshift was explained based on the Cu-Pd alloy formation, which may cause electronic structural change for the valance d bands of Cu and Pd. The signal in the TNT and TNW are much lower than the TNS-based catalysts and hardly distinguished from the background, this may be due to the well incorporation of the Cu inside the morphology of titanium wire

and titanium nanotube which are formed by rolling up the two-dimensional sheets of TiO_2 structure.

The O1s overlapped peaks are resolved into two (2) distinct peaks at around 532 eV and 530.2 eV for all catalyst compositions (Figure 4c). The lower binding energy peak corresponds to the presence of lattice oxygen species [27,33,51] while the peak at around 532 reveals the presence of adsorbed oxygen in hydroxyl species that is present on the surface. Moreover, it can be attributed to carbonate or polarized O^{2-} ions located adjacent to O vacancy sites or to the oxygen in CuO [27,33,51]. According to the literature, the O 1s binding energy of metal hydroxides and metal carbonates are typically around 531.0–531.5 eV [51]. Generally, the peak at the higher binding energy sites only appear in the bimetallic catalysts. This confirms the role of Cu-Pd addition in introducing modification to the oxygen vacancy sites which can play a key role in enhancing CO-oxidation. Furthermore, it can be seen that Pd addition leads to a further upshift of the shoulder peak to a higher binding energy compared to Cu-TNT alone. In our previous study, the O1s peak shifts from 531.5 eV in CuO-TNT to 532.2 in Pd-Cu/TNT in the current study [19]. Similar shift to higher binding energy can be found using TNS support (533.8 eV) and TNW support (532.5 eV). Deconvolution of the O1s peak has been performed for better understanding of the oxygen components (see Figure 6 and Tables S4–S6).
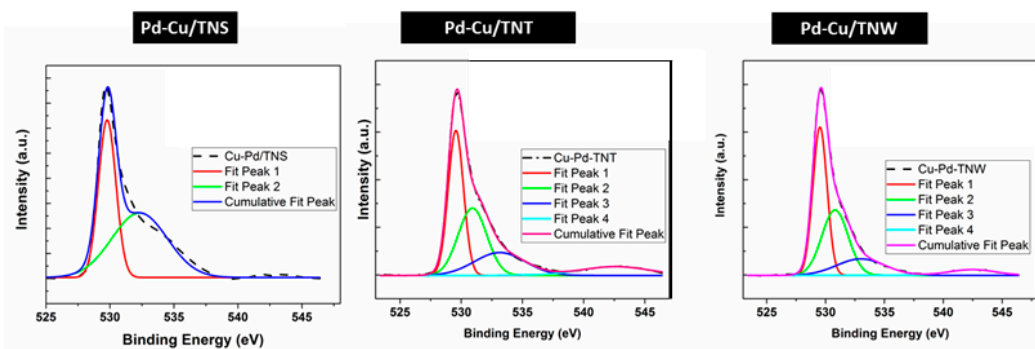

Figure 6. Peak deconvolution for O1s XPS for Pd-Cu/TNS, Pd-Cu/TNT, and Pd -Cu/TNW.

3.5. Vibrational Studies

Figure 7 represents the Raman spectra of the Pd-Cu/TiO_2 nanostructure system synthesized on three different support morphologies namely nanosphere (NS), nanotube (NT), and nanowire (NW) titanium oxide. In addition, the Raman spectra of the pure Cu catalyst on the same supports' morphologies (monometallic systems) were added for comparison. Raman spectra is an important probe tool for the M-O bond environment and the structural changes as those are reflected in the characteristic bands [25,27]. As shown in Figure 7, all the Raman bands are associated with TiO_2 anatase phase. The six active Raman modes of anatase phase are identified as $3E_g$ modes, $1A_{1g}$ mode, and $2B_{1g}$ modes that are attributed to symmetric stretching vibration, antisymmetric stretching vibration, and bending vibration of O-Ti-O, respectively [18,19]. In all the cases of herein catalysts, there is a shift of the position of the main E_{2g} peak to higher wavenumber accompanied by peak broadness. Compared to TiO_2 Eg peak that was reported in our previous study and in the literature, the peak upshifts from 140 cm^{-1} to 143.2 or 142.2 cm^{-1} upon addition of Cu to the support [19,52,53]. The shift becomes more pronounced upon adding the second metal, Pd, to the structure, as the vibrational mode shifts to 147.1 cm^{-1} for Pd-Cu/TNT, Pd-Cu/TNW and to 148.0 cm^{-1} for Pd-Cu/TNS. It is well-known that addition of metal to the support will induce structural change and defects in the crystal. Due to the difference in size of copper ion (Cu^{2+}, 0.7 Å) or palladium ion (Pd^{2+}, 0.7 Å) and Ti^{4+} ions (0.6 Å), TiO_2 lattice structure is anticipated to be distorted following Cu/Pd addition [54]. Furthermore, the charge difference between the copper/palladium and the titanium ion on the substitutional sites will contribute to the structural distortion and lead to oxygen vacancies formation

in the titanium oxide lattice [52,55]. It can be concluded that all the observed upshift in the Raman main E_g peak, can be related to the presence of oxygen vacancies induced by Cu-Pd addition. The presence of oxygen vacancies and surface defects in our study was also confirmed using XPS results (see above Figure 6). According to K. Polychronopoulou et al. phonon confinement and lattice strain upon doping metal on substrate ions can also affect Raman active modes leading to oxygen vacancies generation [28]. The other four important characteristic peaks in the Raman spectra of the prepared catalyst are positioned at 194 cm^{-1} (Eg mode), ~394 cm^{-1} (B$_{1g}$ mode) TiO$_2$ anatase phase, 514 cm^{-1} that is associated with B$_{1g}$+A$_{1g}$ vibrational mode, and 636 cm^{-1} that results from Eg mode [19,56]. These peaks positions were not largely influenced by the addition of the Cu/Pd metals to the support. It is worth mentioning that there is a slightly higher positive shift upon addition of Cu-Pd metals into the titanium oxide in the case of TNW morphology. The peak shifts to 399.68 cm^{-1} (B$_{1g}$) and 639.77 cm^{-1} (Eg) compared to the reported value of TiO$_2$ support alone (at 393 and 636 cm^{-1} respectively) [19,56]. This can clearly show that the morphology of the supports can play a role in the extend of the interaction between the metal and support. The nanowire may provide more exposed surface that can facilitate the degree of Cu-Pd interaction with the support surface.
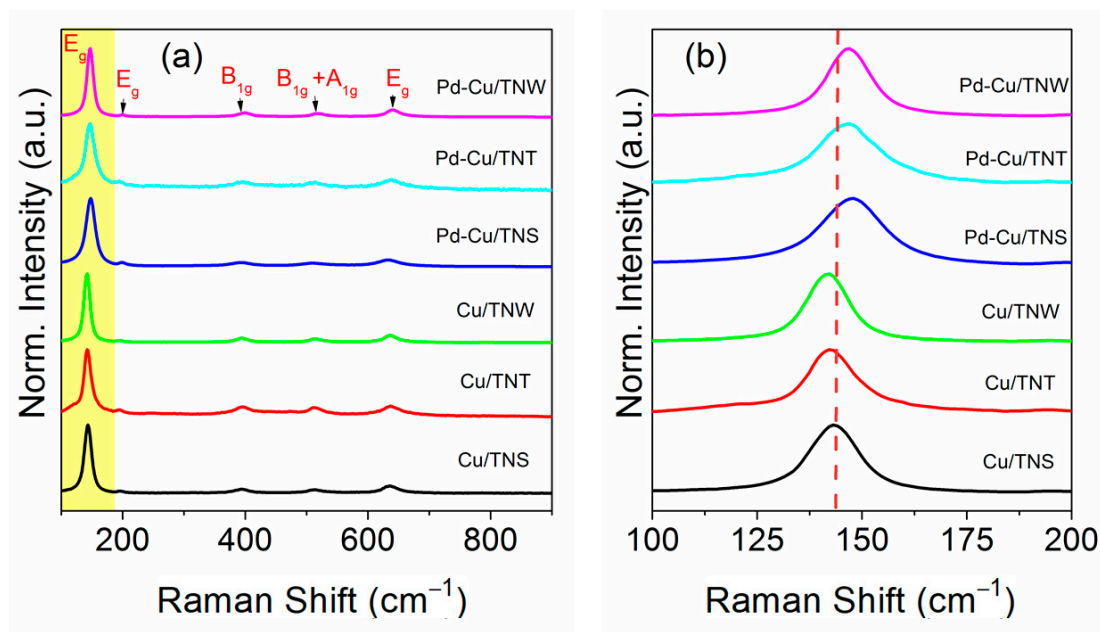

Figure 7. (**a**) Raman spectra of Cu-TNS, Cu-TNT, Cu-TNW, Pd-Cu-TNS, Pd-Cu/TNT, Pd-Cu/TNW catalysts (**b**) Raman spectra of Eg mode of TiO$_2$.

Overall, it can be seen that the TiO$_2$ supports upon Cu and Pd addition facilitates the oxygen vacant sites formation. Furthermore, the absence of any CuO or PdO peak can indicate the fine size of the metal/bimetal. However, it should be mentioned that contradiction between XRD and Raman results in term of PdO presence, could be attributed to the nature of Raman analysis as a surface characterization technique (Raman peak of PdO is masked by the one corresponding to TiO$_2$). The oxygen vacancy creation upon metal addition in TiO$_2$, has been reported in different studies and are in good agreement with our observations [18,30,52,57].

3.6. Catalytic Activity and Stability

The catalytic activity of the different catalysts toward the CO oxidation reaction was measured using a continuous flow fixed-bed catalytic reactor. Figure 8 displays the catalytic activity under the feed gas containing 4% CO and 20% O$_2$ (with Ar as balance).
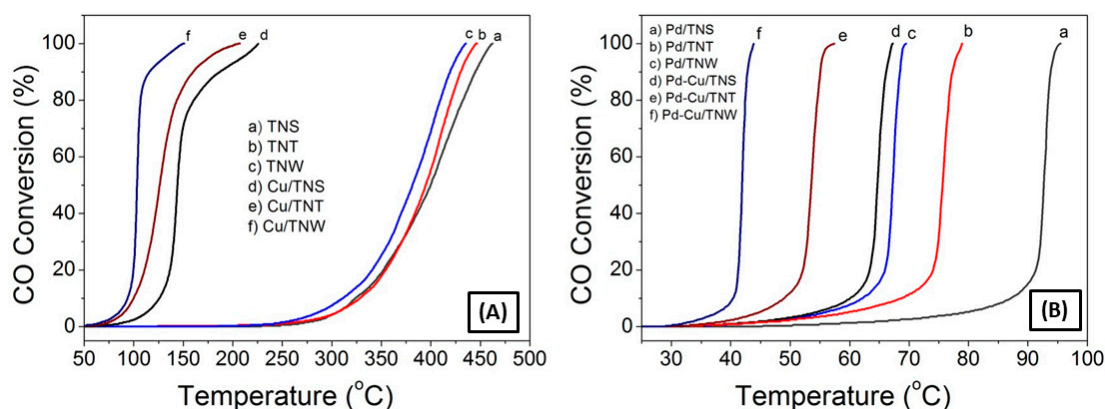
Figure 8. CO oxidation light-off curves of TNS, TNT and TNW support (**A**) before and after Cu loading to the support alone, (**B**) before and after adding Cu to Pd-TiO$_2$ support.

TiO$_2$ bare supports have low CO oxidation activity. As shown in Figure 8A, the different shaped bare TiO$_2$ nanoparticles exhibit a poor catalytic activity toward the oxidation of CO with no significant activity below 300 °C, where the CO oxidation light off curve reveals T$_{50}$ of 399.8 °C, 394.7 °C, and 381.4 °C for TNS, TNT, and TNW, respectively (T$_{50}$ is the corresponding reaction temperature when the conversion is 50%). Our prepared TiO$_2$ nanotube showed a little bit lower activity compared to the TiO$_2$ nanotube prepared by sol-gel and hydrothermal treatment methods, showing T$_{50}$ of 210 °C [1].

When comparing the T$_{50}$ values for the Cu-TiO$_2$ catalysts, it can be seen that, the catalytic activity was significantly increased, with a T$_{50}$ of 144.1 °C followed by T$_{50}$ of 126.2 °C and 103.3 °C for Cu/TNS, Cu/TNT, and Cu/TNW, respectively. This can be attributed to the presence of readily reducible oxygen moieties adjacent to the Cu ion surface. In previous study [19], it was shown that the catalytic activity of CuO-TiO$_2$ NT for CO oxidation is attributed to the interplay between the CuO and TiO$_2$ counterparts and the strong metal–support interaction at the interface. It should be mentioned that Cu is not the only key factor; for the same Cu loading, different oxidation reactivity rates were observed due to the different shapes and microstructure of the supports. The highest catalytic activity was achieved using nanowire support with T$_{50}$ of 103.4 °C and T$_{100}$ of 150.2 °C. This is mostly due to the expected higher surface area along with the uniform distribution of the Cu ion on the TNW support. As a result, the nanowire morphology can lead to more exposed active sites and enhanced activity.

In the case of Pd-based catalyst, further increase in the CO conversion was observed, as reflected by the T$_{50}$ of 92.7 °C, 75.6 °C, and 67.2 °C for the Pd/TNS, Pd/TNT, and Pd/TNW catalysts, respectively. The boost of the activity is reflected onto the T$_{50}$ drop of almost 1.6 times compared to T$_{50}$ of the support alone. This is most likely due to the presence of Pd ions which are widely known to enhance the catalytic activation of CO. Pd metal by itself is a famous CO-oxidation catalyst with high catalytic activity [6,37,58]. However, it was reported that the use of palladium metal alone without using a support will hinder the long-term stability of the catalyst due to metal sintering [7,9,59]. In addition, the high price of this noble metal hinders its use in large-scale application and motivates the study toward the use of support and combination with other cost-effective metals in order to reduce the amount required for such noble metals. Satsuma et al. reported the effect of loading Pd on different supports (CeO$_2$, TiO$_2$, Al$_2$O$_3$, ZrO$_2$, and SiO$_2$) for CO oxidation at low temperatures [60]. The highest CO oxidation was found using CeO$_2$ or TiO$_2$ as a support. A recent publication by the same group has reported a further improvement in the catalyst activity with the use of Pd catalyst supported on titania-coated ceria (T$_{100}$ ~135 °C) [6]. On the other hand, Cheng Hao Wu and his team reported the use of Pd as bimetal system without a support. They reported that CoPd bimetallic nano-catalyst achieved a complete CO conversion at temperature as low as 110 °C and around 180 °C

for Pd catalyst alone [58]. This is still higher temperature compared to our reported Pd on TiO$_2$ (T$_{100}$ = 69.5 °C for Pd/TNW and 95.4 °C in Pd/TNS).

Comparing the catalytic activity of the different catalysts studied in our works, it can be seen that the Pd-Cu catalyst supported on TiO$_2$ exhibit the highest catalytic activity with T$_{50}$ = 64.6 °C for Pd-Cu/TNS, T$_{50}$ = 53.5 °C for Pd-Cu/TNT, and T$_{50}$ = 41.9 °C for Pd-Cu/TNW, so the Pd catalysts modification by nanointerface with Cu and supporting it on TiO$_2$ nanowires demonstrated the highest enhancement in CO oxidation rates with 100% CO conversion at temperature regime down to near-ambient temperatures (T$_{100}$ = 43.85 °C). This result reflects clearly the synergetic effect between Cu, Pd and the TiO$_2$ supports. In addition, a better dispersion of Cu and Pd on the optimized support morphology can provide more population of active site and hence greater CO surface coverage. Overall, it can be stated that the order of catalytic activity toward CO oxidation is as follows TiO$_2$ < Cu/TiO$_2$ < Pd/TiO$_2$ < Pd-Cu/TiO$_2$.

Numerous groups have reported on the CO oxidation activity using similar catalysts system (Table S8). For example, the bimetallic Pd–Cu nano-catalysts have been studied previously in CO oxidation, but using another support, Al$_2$O$_3$. Interestingly, the 100%CO conversion was achieved at higher temperature (200 °C compared to 43.9 °C in our system) [5]. Similarly, Santos et al. reported a range of CO oxidation capacity varying from T$_{50}$ =187 to 413 °C (Pt > Pd ≥ Rh ≈ Ir ≥ Au≥ TiO$_2$), depending on the preparation methods and the noble metal loaded on TiO$_2$ support [61]. Wang et al., have reported that CuO-nanorods-decorated reduced graphene oxide (RGO) nano-catalysts showed total CO oxidation at 165 °C [62], while M. Manolata Devi et al. shows full conversion of CO at 75 °C using Pd-Pt on graphene catalyst [3]. The achieved results are comparable with our system considering that Cu is cheaper in cost and the synthesis method is simpler.

Comparing CO oxidation performance with other affordable yet active systems, such as mixed oxides that were reported in the literature might not be accurate due to the different applied reaction conditions, but generally it indicates that the prepared system in our study has lower T$_{50}$ than different ceria-based oxides e.g., Ce$_x$Sm$_{1-x}$O$_2$ catalysts which are known among the candidates to have great potential for CO oxidation. For example, K. Polychronopoulou reported in their study a minimum of T$_{50}$ = 300 °C for different mixed oxide systems [28]. However, it is worth mentioning that a recent study by Alketbi et al., showed an enhancement in CO oxidation with increasing Cu dopant content (20 at. % Cu) in the Ce-La-Ox catalysts (T$_{50}$ =162 °C). Similarly, a recent study by Akhoori et al. revealed an enhanced CO oxidation activity in samarium-copper co-doped ceria catalysts. The CO oxidation reaction was promoted at low temperature (140 °C) mainly by increasing the Cu content. These studies agree well with our observations of the role of Cu addition in CO oxidation catalytic enhancement [25]. Interestingly, our present catalyst exhibits higher catalytic activity compared to many catalysts in the open literature.

Many factors play a role in controlling the activity of CO oxidation at low temperature. Satsuma et al. indicated in his study of Pd-supported catalyst, that TiO$_2$ can contribute to enhancing the catalyst activity in CO oxidation through the induced reduction–oxidation cycle of supported Pd [6]. In another study, it was found that the role of TiO$_2$ support as an oxygen storage medium and its contribution in oxygen release and storage property, are important factors in enhancing the CO oxidation [60], while equally important is the reducibility degree of the PdO to Pd metal [60]. Mozer and his group reported that addition of Cu to monometallic supported Pd can enhance or suppress the CO oxidation activity depending on the support type [63]. Cu presence reduced the CO oxidation when introduced to Pt/Al$_2$O$_3$ support. This was due to increase in CO desorption rate, as concluded from CO-TPD studies. Also, Cu can block the Pt active site hindering their activity. On the other hand, Cu addition to Pt/Nb$_2$O$_5$ can enhance the CO oxidation activity through improving the metal–metal interaction and Cu contribution in providing additional pathway for O$_2$ adsorption over the reducible Nb$_2$O$_5$ oxide support.

Recently an interesting finding was reported by Polychronopoulou et al. in their study of using different doped ceria oxides in CO oxidation application [64]. The systematic study

demonstrated that heteroatoms substitution will induce lattice distortion but the difference in their activity, can be mainly correlated to the difference in oxygen lattice mobility and the degree of reducibility of the doped metal cation. It was found that Cu doping led to the highest CO oxidation activity due to the high lattice oxygen mobility, synergetic effect between Cu and CeO_2 support, and highest charge compensation in Cu-doped system compared to other heteroatom CeO_2 systems. It should be mentioned that even though CeO_2 and TiO_2 are two different supports however, the governing principle is that by adding different metals at varying loadings leads to the formation of different types of oxygen vacancies (e.g., surface, sub-surface, single, clusters); the latter is what is suggested as a potential scenario in the herein case where Pd-Cu were co-added onto TiO_2. Based on the XRD and Raman findings above, a structural distortion into the TiO_2 lattice occurred most likely due to some incorporation of Cu into titania [$Cu-O-Ti^{4/3}$] in the interface and possible Ov formation. This finding is highly correlated to the activity of the catalysts in CO oxidation, and can be expanded to the exploration of different heteroatom-doped system including TiO_2.

The long-term stability of Pd-Cu/TNW catalyst was evaluated under continuous stream for 72 h as shown in Figure 9. After passing the feed gas mixture over the catalyst, the temperature was increased and maintained at 60 ± 5 °C throughout the whole stability test for CO oxidation. The 100% conversion was rapidly achieved and the performance of the catalyst was continuously maintained during the whole period of study. This indicate that the catalyst is stable and was not subjected to deactivation within the time studied herein. The excellent activity and stability of the Pd-Cu/TNW catalyst enhances the practical value of the catalyst in real-life application.
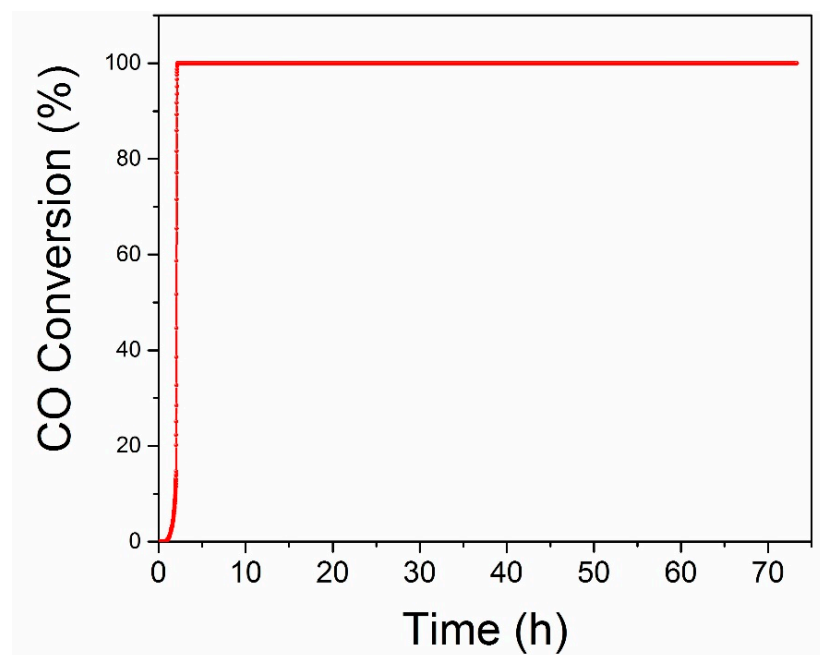

Figure 9. CO oxidation long term stability test of Pd-Cu/TNW under continuous stream for 72 h at ~60 ± 5 °C.

3.7. Mechanistic Aspects of the CO Oxidation Reaction

Different catalytic CO reaction pathways have been proposed in previous studies to explain the catalytic activity toward CO oxidation. Among the proposed mechanisms, Langmuir–Hinshelwood [4,5,65], oxygen spillover [65,66], and Mars van Krevelen mechanisms are suggested as the most popular ones [26,60]. Langmuir–Hinshelwood mechanism was proposed in our previous study as a potential reaction for CO-oxidation, using CuO-TiO_2 nanotube catalyst [19]. This mechanism suggests that both CO and O_2 molecules

are adsorbed on the surface. The CO adsorbs on the metal surface while O_2 adsorbs on the support followed by O_2 dissociation into atomic O. Eventually, the oxidation of the adsorbed CO proceeds through the reaction with the adsorbed O atom. This mechanism was reported recently by Wasim et al. as the leading mechanism in Cu-titanium nanorod catalysts [67]. Several studies in the open literature proposed Langmuir–Hinshelwood mechanism for Cu and Pd supported catalysts as well [19,68]. Fagen Wang proposed that this is mainly applicable for Cu-Pd on Al_2O_3, while more complex mechanisms are expected for TiO_2 [9]. Atsushi Satsuma reported in his study of CO-oxidation over supported Pd catalyst, that titanium oxide contributes to oxygen supply and hence Mars-van Krevelen can be proposed as a more representative mechanism [60]. Mars-van Krevelen is the most prominent mechanism for CO oxidation over different catalysts, such as Cu/Pd-supported catalysts and ceria-based catalysts [24,26,60].

It is well-known that Ti^{3+} formation on the reducible TiO_2 contributes to the formation of the oxygen vacant sites [8,69]. We suggest in our study that CO-oxidation proceeds on Pd-Cu/TiO_2 catalyst by Mars-van Krevelen mechanism. The process has five main steps: (1) Initially, CO molecule chemisorbed on the active metal surface forming Pd-CO; (2) O_2 gas-phase molecule binds at the interface between the support and the active metal surface, in our case O_2 molecule binding to Cu^{2+}/Cu^+ active site was suggested. This step is followed by the dissociation of O_2- and diffusion to the adjacent PdO site [12]; (3) the oxidation of CO by the lattice oxygen at the TiO_2 and Pd-Cu alloy interface leads to the formation of oxygen vacant sites and subsequent reduction of Pd^{2+} to Pd^0; (4) regeneration of the catalysts and continuity of the cycle is proposed to happen through oxygen vacancies interaction with the dissociated O_2 gas-phase molecule; (5) the last step of the mechanism according to Thang and his group, involves oxidation of another CO molecule through the reaction with the extra O atom formed in step 4 [70].

Zhang et al. shows that the strong support interaction and the bifunctional mechanism contribute to the enhanced catalytic activity of Au-Cu supported on CeO_2 [65]. Particularly in the case of bimetal alloy, it was shown that synergistic effect and CO-adsorption-induced surface aggregation are the known phenomena that play a key role in the catalytic activity determination [58,71,72]. In our case, it is believed that Cu will surface segregate and bind to the O_2 gas molecule while Pd will mainly bind to the CO. The reoxidation of the Pd^0 species by Cu^{2+} reduction will ensure the cycle is completed. After that Cu can be easily oxidized using O_2 gas phase molecule. In general, the competition between the CO and O_2 reactants for the binding sites is believed to contribute to the enhanced catalytic activity of the Cu-Pd bimetal supported on the different titanium oxide morphology [12,65]. Proposed CO oxidation pathways over Pd-Cu/TiO_2 catalyst are demonstrated in Figure 10, but in order to verify the mechanism for the promoted activity, more experiments such as in situ DRIFTS studies should be conducted.
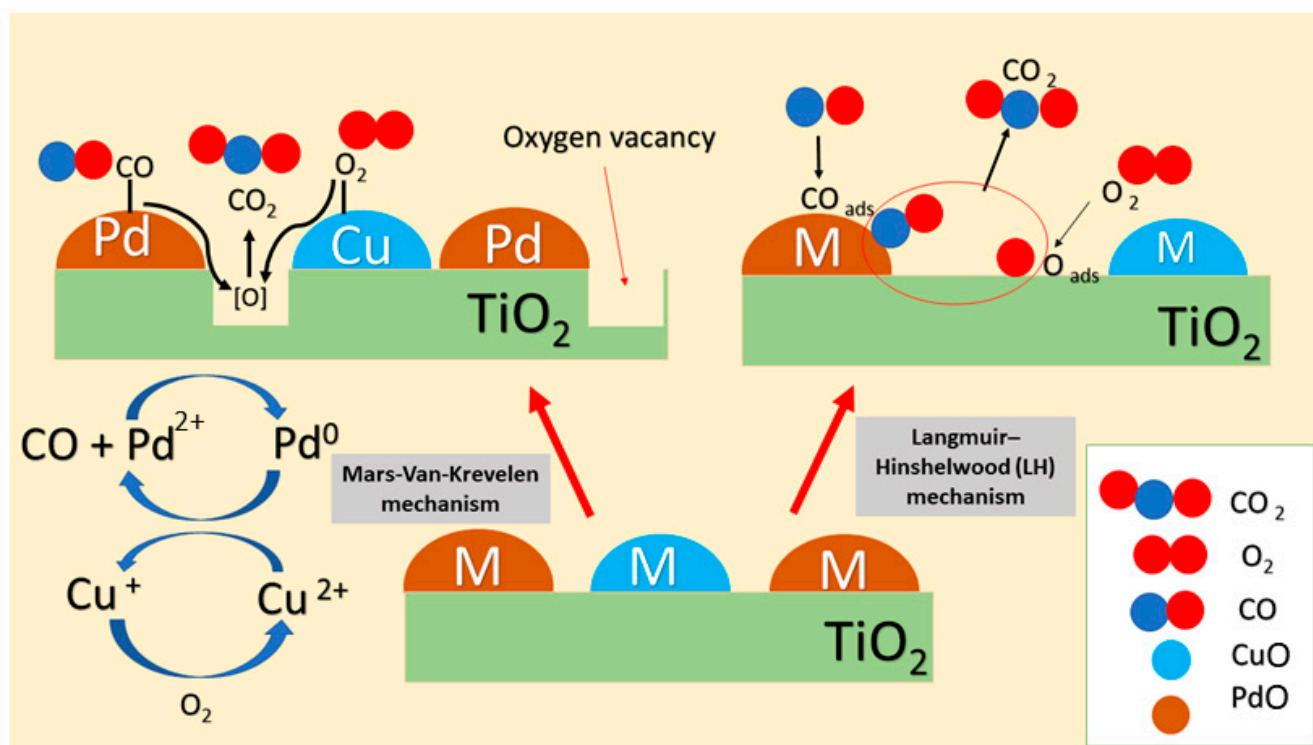
Figure 10. Proposed CO oxidation pathways over Pd-Cu/TiO$_2$ catalyst.

4. Conclusions

In this work, we have demonstrated the promoting effect of the TiO$_2$ support morphologies and the Pd-Cu nano interfacing on the CO oxidation reaction over Pd-Cu/TiO$_2$ catalysts. It was found that the synergy effect between the Cu-Pd and titanium oxide nanowire leads to the most enhanced catalytic activity at lower temperature close to near-ambient conditions. Pd-Cu-based catalysts were developed and supported on three (3) different TiO$_2$ morphology namely nanosphere, nanotube, and nanowire. The results revealed that CO oxidation performance is in the following order TiO$_2$ < Cu/TiO$_2$ < Pd/TiO$_2$ < Pd-Cu/TiO$_2$. It was suggested that the alloying between Cu and Pd metal, facilitate their dispersion in the support. Moreover, nanowire provides more exposed surface with reducible oxygen species and a different anchoring of the Pd, Cu species on it. This led to a considerable improvement in catalytic activity and stability to below 100 °C (T$_{100}$ = 44 °C) using Pd-Cu$^/$TiO$_2$ nanowire. The enhanced interaction between the CO and the oxygen species on the defects sites was correlated and investigated by using different analysis including XRD, Raman, XPS, SEM, and BET physisorption. The development of active oxygen sites was reflected by the up-shift of the E$_{2g}$ mode of TiO$_2$ in the Raman spectrum and the lower binding energy shift of the Ti 2p$_{3/2}$ XPS peak. The understanding presented herein can be extended to tuning other metal–metal oxides interfaces used in the CO oxidation reaction.

References

1. Camposeco, R.; Castillo, S.; Mejía, I.; Mugica, V.; Carrera, R.; Montoya, A.; Morán-Pineda, M.; Navarrete, J.; Gomez, R. Active TiO_2 nanotubes for CO oxidation at low temperature. *Catal. Commun.* **2012**, *17*, 81–88. [CrossRef]

2. Mishra, A.K.; Prasad, R. A Review on Preferential Oxidation of Carbon Monoxide in Hydrogen Rich Gases. *Bull. Chem. React. Eng. Catal.* **2011**, *6*, 1–14. [CrossRef]

3. Devi, M.M.; Dolai, N.; Sreehala, S.; Mishra, R.S.K.; Sharma, S.; Biswas, K.; Jaques, Y.M.M.; Galvao, D.S.; Tiwary, C.S. Morphology controlled graphene–alloy nanoparticle hybrids with tunable carbon monoxide conversion to carbon dioxide. *Nanoscale* **2018**, *10*, 8840–8850. [CrossRef]

4. Zedan, A.F.; Mohamed, A.T.; El-Shall, M.S.; AlQaradawi, S.Y.; AlJaber, A.S. Tailoring the reducibility and catalytic activity of CuO nanoparticles for low temperature CO oxidation. *RSC Adv.* **2018**, *8*, 19499–19511. [CrossRef]

5. Estifaee, P.; Haghighi, M.; Mohammadi, N.; Rahmani, F. CO oxidation over sonochemically synthesized Pd–Cu/Al2O3 nanocatalyst used in hydrogen purification: Effect of Pd loading and ultrasound irradiation time. *Ultrason. Sonochem.* **2014**, *21*, 1155–1165. [CrossRef]

6. Satsuma, A.; Yanagihara, M.; Osaki, K.; Saeki, Y.; Liu, H.; Yamamoto, Y.; Arai, S.; Ohyama, J. Promotion of low-temperature oxidation of CO over Pd supported on titania-coated ceria. *RSC Adv.* **2014**, *4*, 54187–54193. [CrossRef]

7. Duan, D.; Hao, C.; Wang, L.; Shi, W.; Wang, H.; He, G.; Gao, L.; Sun, Z. Rod-Like Nanoporous CeO_2 Modified by PdO Nanoparticles for CO Oxidation and Methane Combustion with High Catalytic Activity and Water Resistance. *Nanoscale Res. Lett.* **2019**, *14*, 199. [CrossRef]

8. Liu, L.; Zhou, F.; Wang, L.; Qi, X.; Shi, F.; Deng, Y. Low-temperature CO oxidation over supported Pt, Pd catalysts: Particular role of FeOx support for oxygen supply during reactions. *J. Catal.* **2010**, *274*, 1–10. [CrossRef]

9. Wang, F.; Zhang, H.; He, D. Catalytic oxidation of low-concentration CO at ambient temperature over supported Pd–Cu catalysts. *Environ. Technol.* **2013**, *35*, 347–354. [CrossRef] [PubMed]

10. Song, C.; Tayal, A.; Seo, O.; Kim, J.; Chen, Y.; Hiroi, S.; Kumara, L.S.R.; Kusada, K.; Kobayashi, H.; Kitagawa, H.; et al. Correlation between the electronic/local structure and CO-oxidation activity of PdxRu1−x alloy nanoparticles. *Nanoscale Adv.* **2018**, *1*, 546–553. [CrossRef]

11. Guo, Z.; Liu, T.; Li, W.; Zhang, C.; Zhang, D.; Pang, Z. Carbon Supported Oxide-Rich Pd-Cu Bimetallic Electrocatalysts for Ethanol Electrooxidation in Alkaline Media Enhanced by Cu/CuOx. *Catalysts* **2016**, *6*, 62. [CrossRef]

12. Ahmad, Y.H.; Mohamed, A.T.; Hassan, W.M.; Soliman, A.; Mahmoud, K.A.; Aljaber, A.S.; Al-Qaradawi, S.Y. Bimetallic palladium-supported halloysite nanotubes for low temperature CO oxidation: Experimental and DFT insights. *Appl. Surf. Sci.* **2019**, *493*, 70–80. [CrossRef]

13. Kumar, R.; Oh, J.-H.; Kim, H.-J.; Jung, J.-H.; Jung, C.-H.; Hong, W.G.; Kim, H.-J.; Park, J.-Y.; Oh, I.-K. Nanohole-Structured and Palladium-Embedded 3D Porous Graphene for Ultrahigh Hydrogen Storage and CO Oxidation Multifunctionalities. *ACS Nano* **2015**, *9*, 7343–7351. [CrossRef] [PubMed]

14. Odoom-Wubah, T.; Du, M.; Osei, W.B.; Sun, D.; Huang, J.; Li, Q. Facile synthesis of porous Pd nanoflowers with excellent catalytic activity towards CO oxidation. *Chin. J. Chem. Eng.* **2015**, *23*, 1907–1915. [CrossRef]

15. Soliman, N. Factors affecting CO oxidation reaction over nanosized materials: A review. *J. Mater. Res. Technol.* **2019**, *8*, 2395–2407. [CrossRef]

16. Samanta, A.; Rajesh, T.; Devi, R.N. Confined space synthesis of fully alloyed and sinter-resistant AuPd nanoparticles encapsulated in porous silica. *J. Mater. Chem. A* **2014**, *2*, 4398. [CrossRef]

17. Bai, Y.; Wang, C.; Zhou, X.; Lu, J.; Xiong, Y. Atomic layer deposition on Pd nanocrystals for forming Pd-TiO_2 interface toward enhanced CO oxidation. *Prog. Nat. Sci.* **2016**, *26*, 289–294. [CrossRef]

18. Carrettin, S.; Hao, Y.; Aguilar-Guerrero, V.; Gates, B.C.; Trasobares, S.; Calvino, J.J.; Corma, A. Increasing the Number of Oxygen Vacancies on TiO2 by Doping with Iron Increases the Activity of Supported Gold for CO Oxidation. *Chem. A Eur. J.* **2007**, *13*, 7771–7779. [CrossRef] [PubMed]

19. Zedan, A.F.; Allam, N.K.; AlQaradawi, S.Y. A Study of Low-Temperature CO Oxidation over Mesoporous CuO-TiO₂ Nanotube Catalysts. *Catalysts* **2017**, *7*, 129. [CrossRef]

20. Yoo, S.J.; Jeon, T.-Y.; Lee, K.-S.; Park, K.-W.; Sung, Y.-E. Effects of particle size on surface electronic and electrocatalytic properties of Pt/TiO2nanocatalysts. *Chem. Commun.* **2010**, *46*, 794–796. [CrossRef] [PubMed]

21. Shi, F.; Baker, L.R.; Hervier, A.; Somorjai, G.A.; Komvopoulos, K. Tuning the Electronic Structure of Titanium Oxide Support to Enhance the Electrochemical Activity of Platinum Nanoparticles. *Nano Lett.* **2013**, *13*, 4469–4474. [CrossRef]

22. Abida, B.; Chirchi, L.; Baranton, S.; Napporn, T.W.; Kochkar, H.; Léger, J.-M.; Ghorbel, A. Preparation and characterization of Pt/TiO2 nanotubes catalyst for methanol electro-oxidation. *Appl. Catal. B Environ.* **2011**, *106*, 609–615. [CrossRef]

23. Youssef, A.; Gad, A.A.E.-E.H.; Ghannam, H.E.-S.; Zedan, A.F.; Aboulthana, W.M.; Al-Sherbini, A.-S. Synthesis of high efficient CS/PVDC/TiO2-Au nanocomposites for photocatalytic degradation of carcinogenic ethidium bromide in sunlight. *Egypt. J. Chem.* **2020**, *63*, 5–9. [CrossRef]

24. Alkhoori, A.; Polychronopoulou, K.; Belabbes, A.; Jaoude, M.A.; Vega, L.F.; Sebastian, V.; Hinder, S.; Baker, M.A.; Zedan, A.F. Cu, Sm co-doping effect on the CO oxidation activity of CeO₂. A combined experimental and density functional study. *Appl. Surf. Sci.* **2020**, *521*, 146305. [CrossRef]

25. AlKetbi, M.; Polychronopoulou, K.; Jaoude, M.A.; Vasiliades, M.A.; Sebastian, V.; Hinder, S.J.; Baker, M.A.; Zedan, A.F.; Efstathiou, A.M. Cu-Ce-La-Ox as efficient CO oxidation catalysts: Effect of Cu content. *Appl. Surf. Sci.* **2020**, *505*, 144474. [CrossRef]

26. Zedan, A.F.; Aljaber, A.S. Combustion Synthesis of Non-Precious CuO-CeO₂ Nanocrystalline Catalysts with Enhanced Catalytic Activity for Methane Oxidation. *Materials* **2019**, *12*, 878. [CrossRef] [PubMed]

27. AlKetbi, M.; Polychronopoulou, K.; Zedan, A.F.; Sebastián, V.; Baker, M.A.; Alkhoori, A.; Jaoude, M.; Alnuaimi, O.; Hinder, S.S.; Tharalekshmy, A.; et al. Tuning the activity of Cu-containing rare earth oxide catalysts for CO oxidation reaction: Cooling while heating paradigm in microwave-assisted synthesis. *Mater. Res. Bull.* **2018**, *108*, 142–150. [CrossRef]

28. Polychronopoulou, K.; Zedan, A.F.; AlKetbi, M.; Stephen, S.; Ather, M.; Katsiotis, M.; Arvanitidis, J.; Christofilos, D.; Isakovic, A.; Alhassan, S. Tailoring the efficiency of an active catalyst for CO abatement through oxidation reaction: The case study of samarium-doped ceria. *J. Environ. Chem. Eng.* **2018**, *6*, 266–280. [CrossRef]

29. Hossain, S.S.; Saleem, J.; Rahman, S.; Zaidi, S.M.J.; McKay, G.; Cheng, C.K. Synthesis and Evaluation of Copper-Supported Titanium Oxide Nanotubes as Electrocatalyst for the Electrochemical Reduction of Carbon Oxide to Organics. *Catalysts* **2019**, *9*, 298. [CrossRef]

30. Garlisi, C.; Scandura, G.; Szlachetko, J.; Ahmadi, S.; Sa, J.; Palmisano, G. E-beam evaporated TiO₂ and Cu-TiO₂ on glass: Performance in the discoloration of methylene blue and 2-propanol oxidation. *Appl. Catal. A Gen.* **2016**, *526*, 191–199. [CrossRef]

31. Etape, E.P.; Ngolui, L.J.; Foba-Tendo, J.; Yufanyi, D.M.; Namondo, B.V. Synthesis and Characterization of CuO, TiO₂, and CuO-TiO₂ Mixed Oxide by a Modified Oxalate Route. *J. Appl. Chem.* **2017**, *2017*, 1–10. [CrossRef]

32. Li, W.; Liang, R.; Hu, A.; Huang, Z.; Zhou, Y.N. Generation of oxygen vacancies in visible light activated one-dimensional iodine TiO₂ photocatalysts. *RSC Adv.* **2014**, *4*, 36959–36966. [CrossRef]

33. Yao, G.; Wu, L.; Lv, T.; Li, J.; Huang, Y.; Dong, K.; Li, X. The effect of CuO modification for a TiO₂ nanotube confined CeO₂ catalyst on the catalytic combustion of butane. *Open Chem.* **2018**, *16*, 1–8. [CrossRef]

34. Khairy, M.; Zakaria, W. Effect of metal-doping of TiO₂ nanoparticles on their photocatalytic activities toward removal of organic dyes. *Egypt. J. Pet.* **2014**, *23*, 419–426. [CrossRef]

35. Wang, Z.-M.; Yang, G.; Biswas, P.; Bresser, W.; Boolchand, P. Processing of iron-doped titania powders in flame aerosol reactors. *Powder Technol.* **2001**, *114*, 197–204. [CrossRef]

36. Imamura, K.; Yoshikawa, T.; Nakanishi, K.; Hashimoto, K.; Kominami, H. Photocatalytic reduction of benzonitrile to benzylamine in aqueous suspensions of palladium-loaded titanium(iv) oxide. *Chem. Commun.* **2013**, *49*, 10911. [CrossRef] [PubMed]

37. Trung, D.D.; Hoang, C.; Van Tong, P.; Van Duy, N.; Dao, T.; Chung, H.; Nagao, T.; Van Hieu, N. Effective decoration of Pd nanoparticles on the surface of SnO₂ nanowires for enhancement of CO gas-sensing performance. *J. Hazard. Mater.* **2014**, *265*, 124–132. [CrossRef]

38. Lisowski, P.; Colmenares, J.C.; Łomot, D.; Chernyayeva, O.; Lisovytskiy, D. Preparation by sonophotodeposition method of bimetallic photocatalysts Pd–Cu/TiO2 for sustainable gaseous selective oxidation of methanol to methyl formate. *J. Mol. Catal. A Chem.* **2016**, *411*, 247–256. [CrossRef]

39. Kumar, M.; Kumar, S.; Kumar, V.; Singh, R. *Growth, Properties, and Applications of β-Ga₂O₃ Nanostructures*; Elsevier: Amsterdam, The Netherlands, 2019; pp. 91–115.

40. De Queiroz, G.A.; Barbosa, C.M.M.D.B. Study of the structural and morphological properties of copper catalysts supported on Al2O3 and TiO2 synthesized by the impregnation method. *Matéria* **2019**, *24*. [CrossRef]

41. Yurdakal, S.; Garlisi, C.; Özcan, L.; Bellardita, M.; Palmisano, G. (Photo)catalyst Characterization Techniques: Adsorption isotherms and BET, SEM, FTIR, UV–Vis, photoluminescence, and electrochemical characterizations. In *Heterogeneous Photocatalysis*; Marcì, G., Palmisano, L., Eds.; Elsevier: Amsterdam, The Netherlands, 2019; Chapter, 4; pp. 87–152. [CrossRef]

42. Tsai, C.-Y.; Hsi, H.-C.; Kuo, T.-H.; Chang, Y.-M.; Liou, J.-H. Preparation of Cu-Doped TiO₂ Photocatalyst with Thermal Plasma Torch for Low-Concentration Mercury Removal. *Aerosol Air Qual. Res.* **2013**, *13*, 639–648. [CrossRef]

43. Deng, C.; Li, B.; Dong, L.; Zhang, F.; Fan, M.; Jin, G.; Gao, J.; Gao, L.; Zhang, F.; Zhou, X. NO reduction by CO over CuO supported on CeO₂-doped TiO₂: The effect of the amount of a few CeO₂. *Phys. Chem. Chem. Phys.* **2015**, *17*, 16092–16109. [CrossRef]

44. Brun, M.; Berthet, A.; Bertolini, J. XPS, AES and Auger parameter of Pd and PdO. *J. Electron Spectrosc. Relat. Phenom.* **1999**, *104*, 55–60. [CrossRef]

45. Yang, G.; Chen, Y.; Zhou, Y.; Tang, Y.; Lu, T. Preparation of carbon supported Pd–P catalyst with high content of element phosphorus and its electrocatalytic performance for formic acid oxidation. *Electrochem. Commun.* **2010**, *12*, 492–495. [CrossRef]

46. Chiba, M.; Thanh, M.N.; Hasegawa, Y.; Obora, Y.; Kawasaki, H.; Yonezawa, T. Synthesis of binary solid solution Cu–Pd nanoparticles by DMF reduction for enhanced photoluminescence properties. *J. Mater. Chem. C* **2014**, *3*, 514–520. [CrossRef]

47. Tian, H.; Zhang, X.L.; Scott, J.; Ng, C.; Amal, R. TiO_2-supported copper nanoparticles prepared via ion exchange for photocatalytic hydrogen production. *J. Mater. Chem. A* **2014**, *2*, 6432–6438. [CrossRef]

48. Biesinger, M.C.; Lau, L.W.; Gerson, A.R.; Smart, R.S. Resolving surface chemical states in XPS analysis of first row transition metals, oxides and hydroxides: Sc, Ti, V, Cu and Zn. *Appl. Surf. Sci.* **2010**, *257*, 887–898. [CrossRef]

49. Meda, L.; Cerofolini, G.F. A decomposition procedure for the determination of copper oxidation states in Cu-zeolites by XPS. *Surf. Interface Anal.* **2004**, *36*, 756–759. [CrossRef]

50. Gao, W.; Chen, J.; Guan, X.; Jin, R.; Zhang, F.; Guan, N. Catalytic reduction of nitrite ions in drinking water over Pd–Cu/TiO_2 bimetallic catalyst. *Catal. Today* **2004**, *93-95*, 333–339. [CrossRef]

51. Polychronopoulou, K.; Zedan, A.F.; Katsiotis, M.; Baker, M.; Alkhoori, A.; AlQaradawi, S.Y.; Hinder, S.; Alhassan, S. Rapid microwave assisted sol-gel synthesis of CeO_2 and CexSm1-xO_2 nanoparticle catalysts for CO oxidation. *Mol. Catal.* **2017**, *428*, 41–55. [CrossRef]

52. Choudhury, B.; Dey, M.; Choudhury, A. Defect generation, d-d transition, and band gap reduction in Cu-doped TiO_2 nanoparticles. *Int. Nano Lett.* **2013**, *3*, 25. [CrossRef]

53. Xue, X.; Ji, W.; Mao, Z.; Mao, H.; Wang, Y.; Wang, X.; Ruan, W.; Zhao, B.; Lombardi, J.R. Raman Investigation of Nanosized TiO2: Effect of Crystallite Size and Quantum Confinement. *J. Phys. Chem. C* **2012**, *116*, 8792–8797. [CrossRef]

54. Sahu, M.; Biswas, P. Single-step processing of copper-doped titania nanomaterials in a flame aerosol reactor. *Nanoscale Res. Lett.* **2011**, *6*, 441. [CrossRef]

55. Shah, M.W.; Zhu, Y.; Fan, X.; Zhao, J.; Li, Y.; Asim, S.; Wang, C. Facile Synthesis of Defective TiO_2-x Nanocrystals with High Surface Area and Tailoring Bandgap for Visible-light Photocatalysis. *Sci. Rep.* **2015**, *5*, 15804. [CrossRef]

56. Chen, C.-A.; Chen, Y.-M.; Huang, Y.-S.; Tsai, D.-S.; Tiong, K.-K.; Liao, P.-C. Synthesis and characterization of well-aligned anatase TiO2 nanocrystals on fused silica via metal–organic vapor deposition. *CrystEngComm* **2009**, *11*, 2313–2318. [CrossRef]

57. Choudhury, B.; Choudhury, A. Dopant induced changes in structural and optical properties of Cr^{3+} doped TiO_2 nanoparticles. *Mater. Chem. Phys.* **2012**, *132*, 1112–1118. [CrossRef]

58. Wu, C.H.; Liu, C.; Su, D.; Xin, H.L.; Fang, H.-T.; Eren, B.; Zhang, S.; Murray, C.B.; Salmeron, M.B. Bimetallic synergy in cobalt–palladium nanocatalysts for CO oxidation. *Nat. Catal.* **2019**, *2*, 78–85. [CrossRef]

59. Davis, M.E.; Lobo, R. Zeolite and molecular sieve synthesis. *Chem. Mater.* **1992**, *4*, 756–768. [CrossRef]

60. Satsuma, A.; Osaki, K.; Yanagihara, M.; Ohyama, J.; Shimizu, K.-I. Activity controlling factors for low-temperature oxidation of CO over supported Pd catalysts. *Appl. Catal. B Environ.* **2013**, *132-133*, 511–518. [CrossRef]

61. Santos, V.P.; Carabineiro, S.A.; Tavares, P.B.; Pereira, M.F.; Órfão, J.J.; Figueiredo, J.L. Oxidation of CO, ethanol and toluene over TiO_2 supported noble metal catalysts. *Appl. Catal. B Environ.* **2010**, *99*, 198–205. [CrossRef]

62. Wang, Y.; Wen, Z.; Zhang, H.; Cao, G.; Sun, Q.; Cao, J. CuO Nanorods-Decorated Reduced Graphene Oxide Nanocatalysts for Catalytic Oxidation of CO. *Catalysts* **2016**, *6*, 214. [CrossRef]

63. Mozer, T.S.; Passos, F.B. Selective CO oxidation on Cu promoted Pt/Al_2O_3 and Pt/Nb_2O_5 catalysts. *Int. J. Hydrog. Energy* **2011**, *36*, 13369–13378. [CrossRef]

64. Polychronopoulou, K.; AlKhoori, A.A.; Efstathiou, A.M.; Jaoude, M.A.; Damaskinos, C.M.; Baker, M.A.; Almutawa, A.; Anjum, D.H.; Vasiliades, M.A.; Belabbes, A.; et al. Design Aspects of Doped CeO_2 for Low-Temperature Catalytic CO Oxidation: Transient Kinetics and DFT Approach. *ACS Appl. Mater. Interfaces* **2021**, *13*, 22391–22415. [CrossRef]

65. Zhang, L.; Kim, H.Y.; Henkelman, G. CO Oxidation at the Au–Cu Interface of Bimetallic Nanoclusters Supported on CeO_2(111). *J. Phys. Chem. Lett.* **2013**, *4*, 2943–2947. [CrossRef]

66. Vayssilov, G.N.; Lykhach, Y.; Migani, A.; Staudt, T.; Petrova, G.P.; Tsud, N.; Skála, T.; Bruix, A.; Illas, F.; Prince, K.C.; et al. Support nanostructure boosts oxygen transfer to catalytically active platinum nanoparticles. *Nat. Mater.* **2011**, *10*, 310–315. [CrossRef] [PubMed]

67. Khan, W.U.; Chen, S.S.; Tsang, D.; Teoh, W.Y.; Hu, X.; Lam, F.L.Y.; Yip, A.C.K. Catalytically active interfaces in titania nanorod-supported copper catalysts for CO oxidation. *Nano Res.* **2020**, *13*, 533–542. [CrossRef]

68. Lu, J.-Q.; Sun, C.-X.; Li, N.; Jia, A.-P.; Luo, M.-F. Kinetic study of CO oxidation over CuO/MO_2 (M = Si, Ti and Ce) catalysts. *Appl. Surf. Sci.* **2013**, *287*, 124–134. [CrossRef]

69. Maynes, A.J.; Driscoll, D.M.; Desario, P.A.; Pietron, J.J.; Pennington, A.M.; Rolison, D.R.; Morris, J.R. Electronic Metal–Support Interactions in the Activation of CO Oxidation over a Cu/TiO_2 Aerogel Catalyst. *J. Phys. Chem. C* **2020**, *124*, 21491–21501. [CrossRef]

70. Thang, H.V.; Pacchioni, G. CO oxidation promoted by a Pt4/TiO_2 catalyst: Role of lattice oxygen at the metal/oxide interface. *Catal. Lett.* **2019**, *149*, 390–398. [CrossRef]

71. Goulas, K.A.; Sreekumar, S.; Song, Y.; Kharidehal, P.; Gunbas, G.; Dietrich, P.J.; Johnson, G.R.; Wang, Y.C.; Grippo, A.M.; Grabow, L.C.; et al. Synergistic Effects in Bimetallic Palladium–Copper Catalysts Improve Selectivity in Oxygenate Coupling Reactions. *J. Am. Chem. Soc.* **2016**, *138*, 6805–6812. [CrossRef] [PubMed]
72. Ab Aziz, M.A.; Setiabudi, H.D.; Teh, L.P.; Asmadi, M.; Matmin, J.; Wongsakulphasatch, S. High-Performance Bimetallic Catalysts for Low-Temperature Carbon Dioxide Reforming of Methane. *Chem. Eng. Technol.* **2020**, *43*, 661–671. [CrossRef]